JOURNAL OF PROPULSION AND POWER
Vol. 16, No. 3, May–June 2000

Experimental Investigation of Rotor-Inlet Guide Vane Interactions in Transonic Axial-Flow Compressor

Albert J. Sanders* and Sanford Fleeter†
Purdue University, West Lafayette, Indiana 47907

Experiments are performed in an advanced-design multistage axial-flow compressor to investigate rotor-inlet guide vane (IGV) unsteady aerodynamic blade-row interaction phenomena at both transonic and subsonic rotor operating conditions. Nonlinear interaction effects were significant at the transonic design speed, with very high levels of unsteady loading occurring in the vane trailing edge region because of interactions with the rotor-generated shock waves. The impact of these shocks with the vane pressure surface resulted in a reflected shock segment that traveled across the vane passage as it propagated upstream, eventually impacting the suction surface of the adjacent vane. Increasing the IGV-rotor axial spacing did not significantly reduce the unsteady aerodynamic loading caused by these interactions, with harmonics as high as 8 × blade pass frequency still present in the vane response. These nonlinear interactions did not occur at the part-speed operating condition in which the rotor flow was subsonic, with both the forcing function and vane response predominantly first harmonic.

Nomenclature

C = inlet guide vane chord
f = frequency
f_{BP} = blade-pass frequency
N_c = corrected rotor speed
P_t = time–average inlet total pressure
p = airfoil surface static pressure
p_s = forcing function static-pressure fluctuation
T_{BP} = blade-pass period
t = time
x = chordwise location
Δp = airfoil unsteady pressure difference, $p_{ps} - p_{ss}$

Subscripts

ps = airfoil pressure surface
ss = airfoil suction surface

Introduction

TO meet the demands of higher thrust-to-weight ratios and reduced fuel consumption, the current trends in aircraft engine compressor designs are toward higher tip speeds, higher airfoil loading, more closely spaced blade rows, and fewer stages. As a result, these advanced design compressors generally feature thin low-aspect ratio airfoils that are highly susceptible to flow-induced vibrations. The driving phenomena for these flow-induced vibrations are the unsteady aerodynamics, with high cycle fatigue (HCF) a universal problem throughout the gas turbine industry. In fact, the loss of blades, vanes, and disks because of HCF is the predominant surprise engine failure mode in the field, with both mature and new engine and blading designs experiencing HCF.

The prediction of blade-row interaction phenomena in transonic compressors is most challenging because of nonlinear aerodynamic and strong blade-row coupling effects resulting from the highly unsteady nature of the flowfield. When the axial velocity component is subsonic, shock waves are formed near the leading edges of the rotor blades, which propagate upstream into the neighboring inlet guide vane (IGV) row (Fig. 1). The upstream vane surfaces reflect and diffract these incident shock waves in a complex manner, with a time-dependent wave pattern established in the upstream vane passages caused by the periodic interaction process. Because turbomachine stages generally feature unequal vane-blade counts, these IGV-rotor interactions vary from passage-to-passage around the annulus of the compressor at any given instant in time.

Eulitz et al.[1] investigated the response of an upstream stator to shocks generated by the downstream rotor in a transonic compressor using two-dimensional viscous and inviscid analyses. The inviscid analysis of three stator and two rotor passages indicated that the rotor shocks interacted strongly with the upstream vane trailing edges, reflecting off the vane surfaces multiple times as they propagated upstream through the vane passage. Fourier analysis of the vane surface-pressure distributions indicated that the first harmonic-pressure fluctuations caused by this interaction were as large as 10% of the time-average values, with significant second and third harmonics also present.

Viscous calculations using a one-equation turbulence model were performed with the geometry scaled such that each airfoil row was represented as a single passage. This pitch ratio change had a dramatic effect on the reflected wave pattern in the upstream vane row. These wave reflections induced unsteady flow separation on both airfoil surfaces, with separation bubbles evolving and vanishing over a single blade-passing period. This flow separation was most significant on the vane suction surface, with the shock-induced separation zone encompassing almost 40% chord before it reattached about halfway through the cycle.

Liamis et al.[2] analyzed transonic IGV-rotor interactions using a quasi-three-dimensional Navier–Stokes analysis and reported similar results. Namely, the rotor leading-edge shock waves generated a reflected wave pattern in the upstream vane passages, with the incident shocks eventually degenerating into pressure waves as they propagated upstream through the vane row. This interaction caused the IGV outlet flow angle and velocity to vary significantly over one blade-passing period, with the outlet flow angle experiencing fluctuations of up to 8 deg.

Arnone and Pacciani[3] analyzed IGV-rotor interactions in the tip section of a transonic compressor stage using a two-dimensional Navier–Stokes analysis, with the unsteady simulations performed for several mass flow rates ranging from choke to near stall. The rotor bow shock was reflected by the upstream IGVs back toward the rotor, with these reflections becoming much stronger as the mass-flow rate through the stage was reduced. At the near-stall operating condition, the impact of the shock with the upstream vane trailing

Received 14 August 1998; revision received 28 April 1999; accepted for publication 4 June 1999.

*Research Assistant, School of Mechanical Engineering, 1003 Chaffee Hall. Student Member AIAA.

†McAllister Distinguished Professor, School of Mechanical Engineering, 1003 Chaffee Hall. Associate Fellow AIAA.

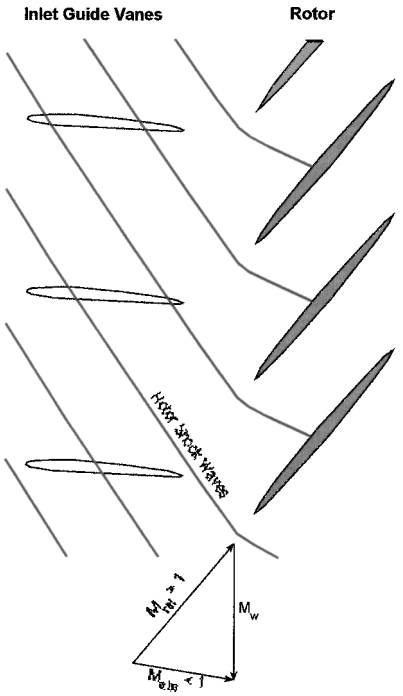

Fig. 1 IGV excitation caused by rotor leading-edge shock waves.

edge caused a large eddy to form, which convected downstream and was ingested into the rotor passage.

Time-accurate computational fluid dynamics (CFD) analyses are being utilized to analyze nonlinear blade-row interactions in advanced turbomachine designs. However, these solutions are dependent upon the particular turbulence model utilized, with the computational domain also reduced by scaling the geometry such that each airfoil row is represented at most by a few passages. This greatly reduces storage requirements but alters the fundamental periodicity of rotor-stator interactions, i.e., the interblade phase angle specified by the blade-vane count ratio. Fundamental blade-row interaction data are thus needed to assess the validity of these CFD analyses.

This paper addresses this need, with detailed benchmark IGV-rotor unsteady aerodynamic blade-row interaction data acquired in an advanced design transonic multistage research compressor. These detailed data include measurements of the rotor-generated forcing function and the resultant IGV response in the tip region of the compressor resulting from transonic interactions. These measurements are made at several steady operating points defined on the compressor map, with the effects of axial spacing and part-speed operation also investigated.

Research Facility

The Purdue Transonic Multistage Research Compressor features a one-and-one-half-stage axial-flow geometry, which is representative of that used in the front stages of advanced aircraft engine high-pressure compressor designs. The drive system consists of a 400 horsepower AC motor, a variable speed magnetic clutch, and an 8:1 ratio gearbox, the output of which drives the compressor rotor (Fig. 2). Atmospheric air is drawn into the test section through a converging bellmouth inlet with a 16:1 contraction ratio and exits the test section through discharge piping, which contains a butterfly throttle valve to regulate the flow rate.

The test section has a constant hub-tip ratio of 0.67 with a tip diameter of 0.3 m (12.0 in.) and features an IGV row, a blisk with 19 rotor blades, and a downstream stator. The compressor design speed is 20,000 rpm, with a maximum pressure ratio of 1.38. The rotor blades consist of NACA 65 series profiles on circular arc meanlines with a 5.08-cm (2.0-in.) chord and a thickness distribution varying from 10% at the root to 6% at the tip. The IGV and stator vanes are an advanced controlled diffusion airfoil (CDA) design with a 4.45-cm (1.75-in.) chord and a constant 7% thickness. Both the IGV row and stator feature variable stagger angles, adjustable axial spacings, and can be independently configured with either 18 or 20 vanes. Additionally, the IGV row is indexable, thereby permitting vane-row clocking effects to be investigated, i.e., the IGV ring can be clocked circumferentially relative to the downstream stator and stationary instrumentation probes.

Data Acquisition and Analysis

Measurements of the rotor-generated unsteady aerodynamic forcing function and the resultant IGV steady and unsteady surface-pressure distributions are made at 90% span at several operating points on the compressor map. An unsteady static-pressure probe is used to measure the potential flow-generated forcing function upstream of the rotor, with vane mounted high-response Kulite XCS-093 5 psi sealed gauge pressure transducers used to measure the resultant IGV response. These transducers are reverse mounted within the suction surface of one vane and the pressure surface of an adjacent vane, with the chordwise tap locations shown in Fig. 3. Preliminary CFD analysis performed during the compressor design indicated that the rotor operates with a single detached leading-edge shock wave, which is a significant source of unsteady aerodynamic excitation to the upstream IGV. Thus, the transducers are concentrated along the aft region of the IGV because this is where strong interactions with the rotor-tip shock system are expected. To minimize probe interference effects, the unsteady static-pressure probe is located 21.4% vane chord downstream of the IGV and circumferentially positioned at 44.55% pitch between the trailing edges of the vanes adjacent to the instrumented passage (Fig. 3).

Very large unsteady pressures on the vane surfaces exceeding the quoted linearity range of the transducers are to be measured. Consequently, the transducers were statically calibrated over a pressure range from 0–7 psi, with the sensitivity found to be nearly linear over this pressure range. Accounting for nonlinearities, the maximum uncertainty in the unsteady pressure measurements is estimated to be 0.5%, with the frequency responses estimated to be 50 and 70 kHz for the unsteady static-pressure probe and instrumented vanes, respectively.

The bridge voltage to the pressure transducers is provided with a Syminex M1000 24-channel signal conditioning unit, with M1064 high-bandwidth AC coupled amplifiers used to condition the signals. The instantaneous amplified signals are simultaneously recorded along with a once-per-revolution pulse from a shaft mounted photo-optic sensor on analog tape using a TEAC XR9000 Super High Band 28 channel VHS Data Recorder. Approximately 20,000 revolutions (one min) of data are recorded at a tape speed of 76.2 cm/s (30 in./s) for each operating point, with the frequency response of the recorder 80 kHz for this tape speed.

The data are processed off-line, with the signals digitized at a rate of 1 MHz and phase-lock averaged over 500 revolutions using the once-per-revolution signal as the data initiation pulse. These digitized signals are shifted in the time domain to represent the time-variant flowfield of a single IGV passage, with 24 rotor blade-passing periods (1.26 revolutions) of phase-lock averaged data for this reference passage stored to disk for subsequent analysis. The vane-blade initial position for these data correspond to the rotor stacking axis being at the center of the reference passage at time $t = 0$. For the data presented herein the phase-lock averaged surface pressure waveforms for the lower vane have also been shifted to represent the time-variant flowfield on the upper vane in the reference passage, i.e., a single equivalent airfoil. The forcing function measurements are not shifted and lead the measurements at the upper vane trailing edge by 58.5% of a blade-pass period.

Results

The unsteady aerodynamic IGV-rotor interactions are investigated at several steady compressor loading conditions, including the effect of design (transonic) and part-speed (subsonic) rotor operation and IGV-rotor axial spacing. For these experiments the IGV and stator are each configured with 18 vanes set at their design stagger angles (minimum loss incidence). The IGV row is fixed in the unclocked position, i.e., the stacking axes of the IGV and

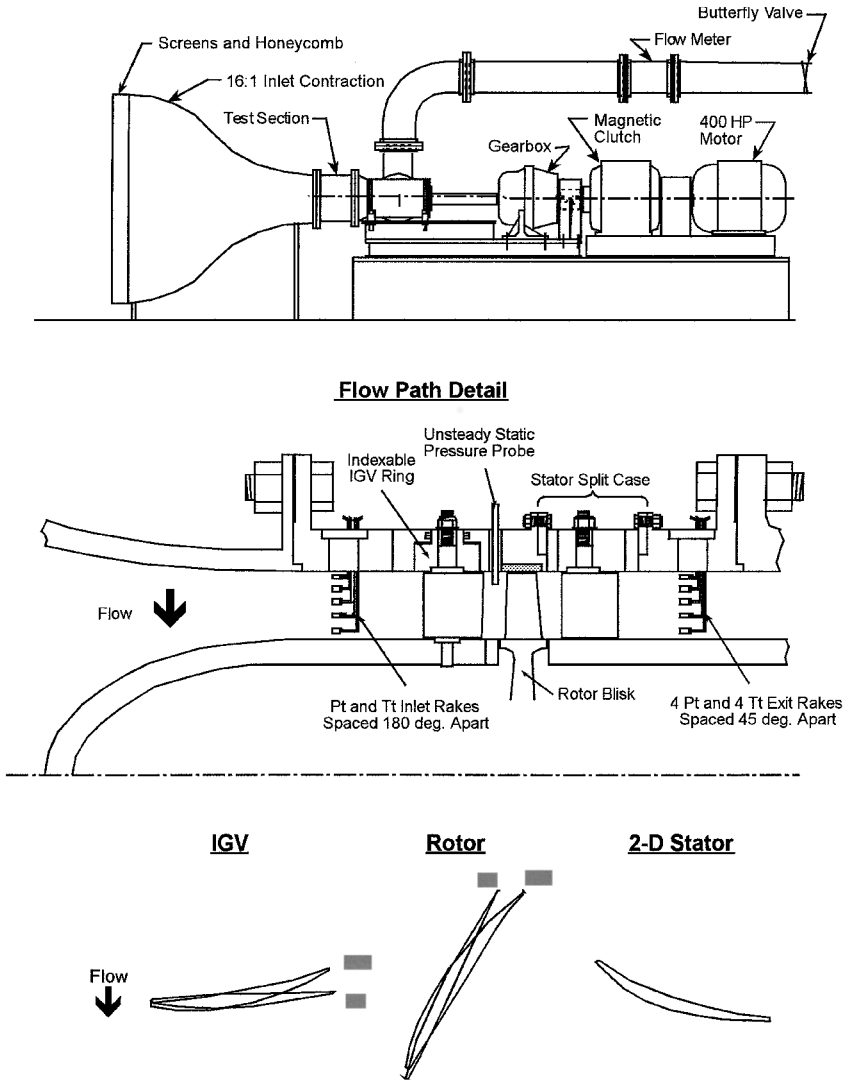

Fig. 2 Purdue Multistage Transonic Compressor Research Facility.

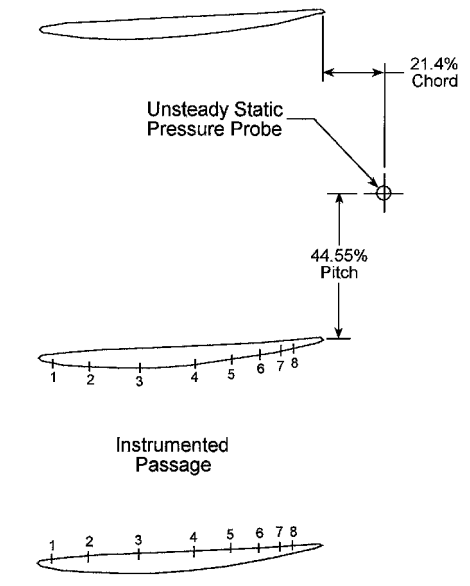

Tap No.	1	2	3	4	5	6	7	8
% Chord	5.0	17.5	35.0	55.0	67.5	77.5	85.0	90.0

Fig. 3 90% span instrumentation locations.

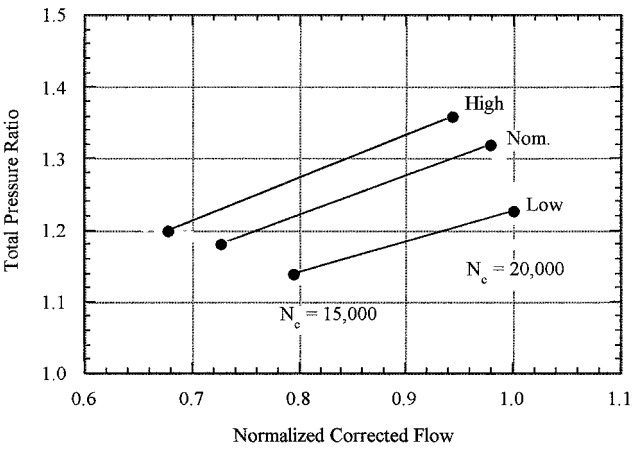

Fig. 4 Purdue Transonic Multistage Compressor Performance Map.

stator vanes coincide at the same circumferential position (Fig. 2). Unless otherwise noted, the baseline compressor geometry features moderate axial spacings, i.e., the IGV-rotor and rotor-stator midspan axial spacings are set at 41.4 and 39.0% vane chord, respectively.

Measurements of the baseline compressor performance define the operating points at which the detailed unsteady aerodynamic data are acquired (Fig. 4). Data are acquired along three operating lines at 75% ($N_c = 15{,}000$ rpm) and 100% ($N_c = 20{,}000$ rpm) design

speed. These operating lines correspond to low steady loading, nominal loading at the aerodynamic design point, and a highly loaded condition near the compressor stall boundary.

Rotor-Generated Forcing Function

The effect of steady compressor loading on the rotor-generated unsteady static-pressure field, i.e., the forcing function to the upstream IGV, is shown in Fig. 5 for both design (transonic) and part-speed (subsonic) rotor operating conditions. Presented is the time-variant static pressure nondimensionalized by the time-average inlet total pressure, with time nondimensionalized by the blade-pass period. Note that the scales are different, with the maximum static-pressure fluctuations at the transonic operating conditions three-and-one-half times larger than those for subsonic rotor flow.

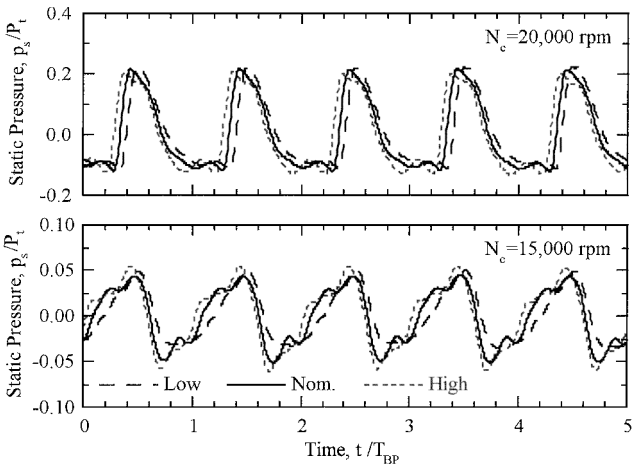

Fig. 5 Effect of steady loading on rotor-generated forcing function.

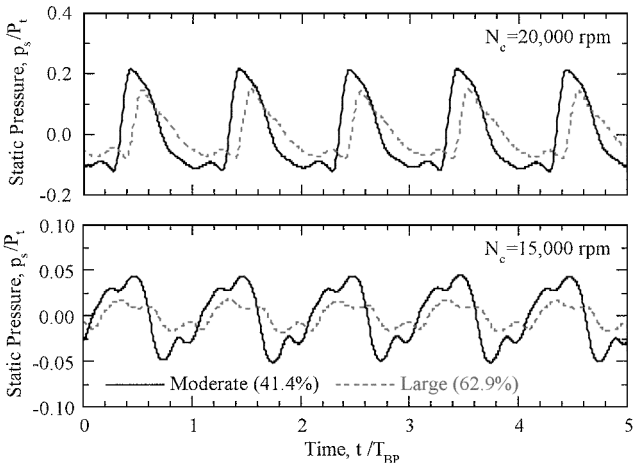

Fig. 6 Effect of axial spacing on rotor-generated forcing function.

These pressure fluctuations are very large, with peak-to-peak amplitudes to 35 and 10% of the inlet total pressure for the transonic and subsonic rotor speeds, respectively. The very large fluctuations at the transonic design speed are caused by the shock waves generated by the rotor. Note that the forcing functions generated by subsonic rotor operation are by no means insignificant. Rather, they are small only in comparison to those generated at the transonic operating condition. Notice also that the waveforms are significantly different, transitioning from a sawtooth-type pattern for subsonic rotor flow to a series of large amplitude periodic pulses at the transonic design speed. However, steady compressor loading does not have a strong effect on the forcing function, with the maximum amplitudes nearly identical for all operating conditions.

The effect of axial spacing on the rotor-generated forcing function is shown in Fig. 6 for the nominal operating line. For these data the IGV-rotor midspan axial spacing was increased to 62.9% vane chord while the rotor-stator axial spacing was unchanged. Because the data are acquired at the same axial location relative to the IGV trailing edge for both axial spacings, this figure shows the decay characteristics of the unsteady aerodynamic forcing function generated by the rotor.

Increasing the axial spacing causes the strength of the static-pressure fluctuation to decrease for both transonic and subsonic operating conditions. For the transonic design speed, the peak-to-peak static-pressure fluctuation decreases nearly 30% as the axial spacing is increased, with this decay attributed to nonlinear dissipation mechanisms. For the subsonic part-speed operating condition the decay of the rotor potential field is much more pronounced, with the peak-to-peak pressure fluctuation decreasing nearly 60% for the increased axial spacing.

IGV Unsteady Aerodynamic Response

Because of the axial inlet flow, the IGV row operates at minimum loss incidence with nearly the same level of steady loading for all operating conditions investigated in these experiments. Additionally, the amplitude of the rotor-generated forcing function to the IGV is not strongly affected by changes in the compressor loading. Thus, the detailed IGV response is only investigated at the nominal operating condition, with the effects of subsonic and transonic rotor operation as well as IGV-rotor axial spacing quantified.

The unsteadiness on the IGV surfaces is shown in Fig. 7. Specifically, the vane surface unsteady pressure envelopes along with the

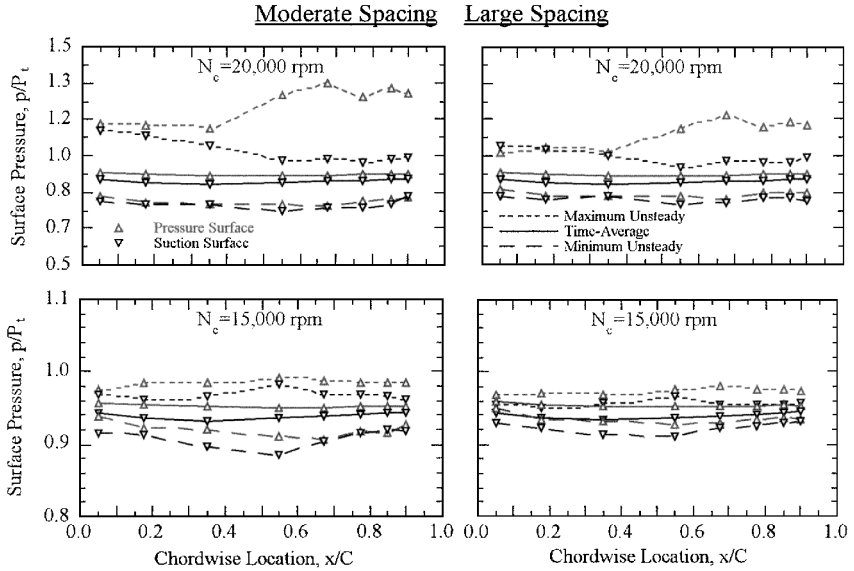

Fig. 7 Unsteady IGV pressure envelopes.

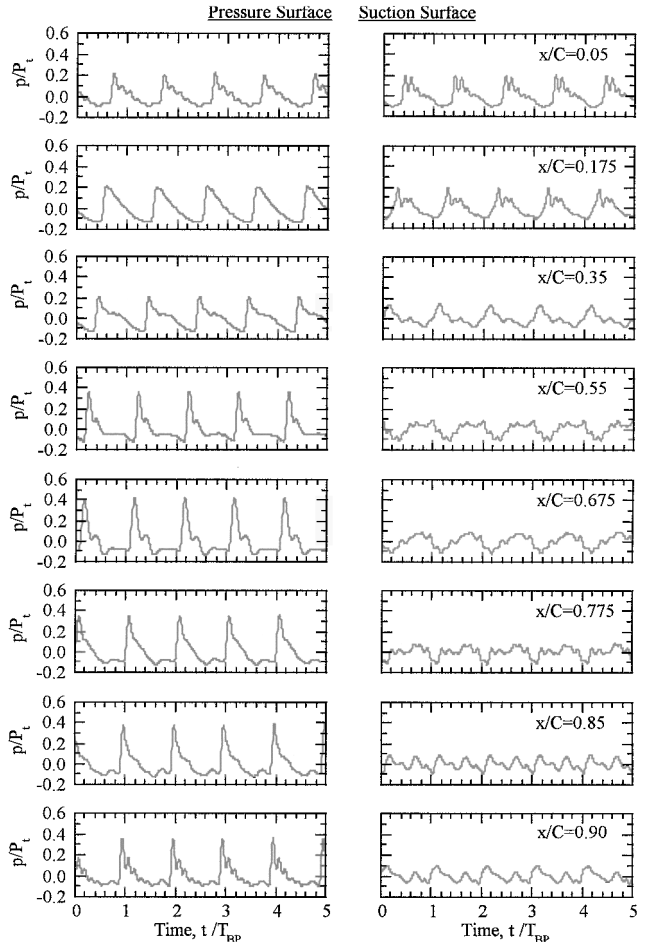

Fig. 8 IGV surface-pressure waveforms at 20,000 rpm (moderate axial spacing).

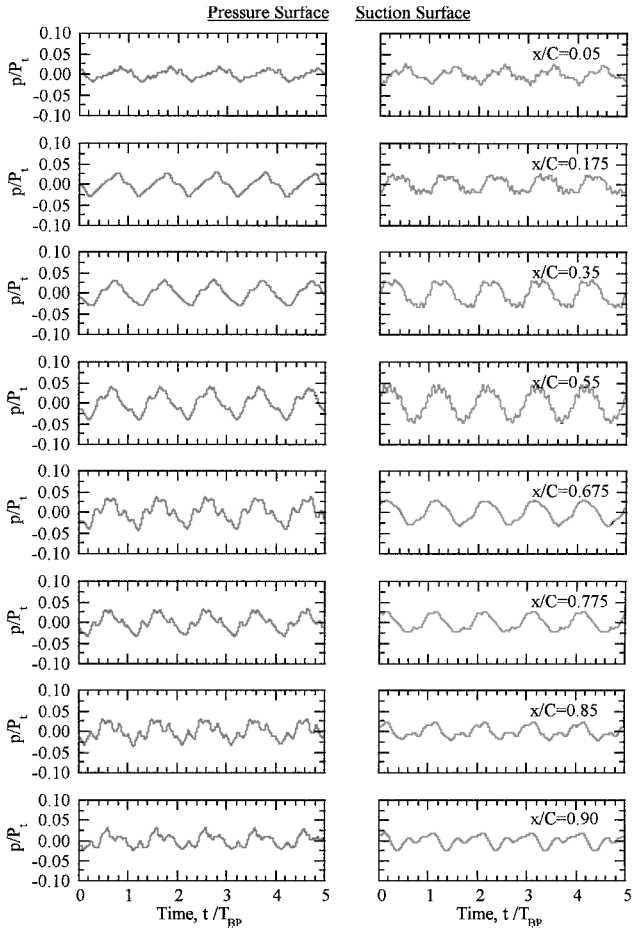

Fig. 9 IGV surface-pressure waveforms at 15,000 rpm (moderate axial spacing).

time-average pressure distributions for the moderate and large axial spacings at the transonic and subsonic rotor operating conditions are shown.

At the transonic design speed the maximum unsteady pressure surface loading is highest along the aft 30% chord, decreasing as one moves forward from 70 to 30% chord, and then remaining relatively constant over the front 30% of the chord. Note that the suction surface exhibits the opposite trend, with the unsteady loading highest near the leading edge, decreasing in a nearly linear fashion to 60% chord, and then remaining nearly constant over the aft 40% chord. This unsteadiness is very significant, reaching amplitudes as high as 60% (maximum–minimum) of the inlet total pressure in the trailing-edge region at the moderate spacing. Increasing the axial spacing reduces the magnitude of the unsteady loading, but the loading still reaches levels as large as 40% of the inlet total pressure, which corresponds to nearly one-half of the steady loading in the trailing-edge region. Also note that the vane suction surface unsteadiness begins to increase at approximately the same chordwise location as that at which the pressure surface unsteadiness begins to decrease, with the unsteadiness the same order of magnitude near the vane leading edge on both vane surfaces.

The unsteady vane loading is considerably reduced at the subsonic rotor operating condition, with the maximum peak-to-peak pressure fluctuations at the moderate spacing only around 10% of the inlet total pressure. Additionally, the pressure fluctuations are highest over the central portion of the vane on both airfoil surfaces. This is in contrast to the transonic rotor speed data where the fluctuations were highest in the vane pressure surface trailing-edge and suction surface leading-edge regions. Because the forcing function generated by subsonic rotor operation decays exponentially with axial distance, the vane response might be expected to be highest in the IGV trailing-edge region at this operating condition. The data, however, indicate that the unsteadiness is the same order of magnitude in the vane leading- and trailing-edge regions and highest over the central portion of the vane. This can be caused by acoustic phenomena, with IGV-rotor interactions generating acoustic modes that propagate upstream through the vane passage. These acoustic modes are contained in both the forcing function and vane response data because they occur at multiples of blade-pass frequency and are phase-locked to the rotor. The forcing function generated in the transonic regime is three-and-one-half times larger than that generated by subsonic rotor operation. However, the maximum unsteady loading on the IGV at the design speed as a result of this interaction is six times larger than that at part-speed. We will show that this dramatic increase in unsteady loading at transonic speeds is caused, in part, by nonlinear interaction effects in the vane trailing-edge region, with these effects not present for subsonic rotor operating conditions.

Figures 8 and 9 show the vane surface time-variant AC coupled pressures used to construct the unsteady envelopes for the moderate axial spacing at transonic and subsonic rotor operating conditions. At the transonic design speed the waveform on both vane surfaces changes noticeably with chordwise location. In fact, the waveform change with chordwise location correlates very well with the changes in amplitude noted for the unsteady envelopes. In particular, the pressure surface fluctuations are very sharp and impulsive over the aft 30% of the vane where the rotor generated unsteadiness is largest. The waveform, however, transitions to a sawtooth-type pattern over the central portion of the vane as the unsteadiness attenuates, then becoming uniform again over the front one-third of the chord. A similar trend is apparent on the suction surface, with the waveform changing noticeably along the chord as the unsteadiness increases from the trailing to the leading edge.

Upstream propagating wave phenomena are clearly evident on the vane pressure surface, with the maximum pressure fluctuations

occurring at later times as waves propagate upstream along the vane chord. The pressure and suction surface waveforms are also noticeably different at the vane trailing edge, but become very similar to one another near the leading edge. The surface-pressure fluctuations are in phase at the trailing edge but nearly 180 deg out of phase at the leading edge. This indicates that a time-dependent wave phenomenon is established in the vane passage because of its interaction with the downstream rotor.

Analogous results are presented in Fig. 9 for the part-speed subsonic rotor operating condition. The waveform changes with chordwise location again correlate with the amplitude changes of the unsteady pressure envelopes, but are not as dramatic as those noted for transonic rotor operation. On both vane surfaces the waveform is nearly sinusoidal over the front half chord, with the amplitudes nearly identical but the fluctuations sharper on the pressure surface. As the trailing edge is approached, the amplitude of the unsteadiness attenuates, and the waveforms become more erratic, most notably on the pressure surface. The wave phenomena observed at the transonic design speed are no longer present, with the maximum pressure fluctuations on each vane surface occurring at nearly the same time for all chordwise locations. Additionally, the fluctuations on each surface are nearly 180 deg out of phase along the entire chord, in contrast to the trend noted for the transonic rotor speed.

Instantaneous IGV Pressure Distributions

To gain insight into the evolution of the unsteadiness, the instantaneous IGV surface-pressure distributions generated at the rotor transonic design speed over one periodic cycle are examined. Figure 10 shows the phase-lock averaged surface-pressure distributions at 10 equally spaced increments over one blade-pass period for the moderate axial spacing. Also shown for reference in the center of Fig. 10 is the rotor-generated unsteady aerodynamic forcing function. Recall that this forcing function is measured at approximately midpitch and leads the measurements at the reference vane trailing edge by 58.5% of the blade-pass period. To compensate for this time delay, the pressure fluctuations associated with the passing of the rotor shock at each time increment are indicated on the forcing function waveform by the open symbols for one vane response cycle.

Upstream travelling wave phenomena are clearly evident on both vane surfaces, with the pressure and suction surface responses nearly 180 deg out of phase along most of the chord. This behavior is attributed to a time-dependent wave pattern being generated in the IGV passage caused by the interaction of the rotor shock waves with the upstream vane row. The rotor shocks periodically impact the trailing-edge region of the upstream vanes, with a reflection of the incident shock wave occurring on the pressure (upper) surface and diffraction occurring on the suction (lower) surface as the shock bends around the trailing edge (Fig. 11).

The reflection of the shock by the vane pressure surface causes a significant increase in the static pressure (overpressure zone) to

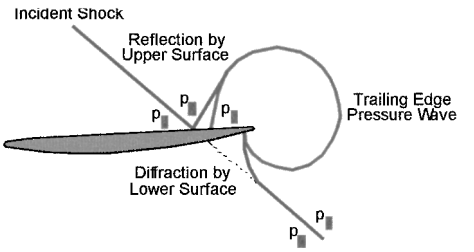

Fig. 11 Shock-wave interaction with an isolated vane.

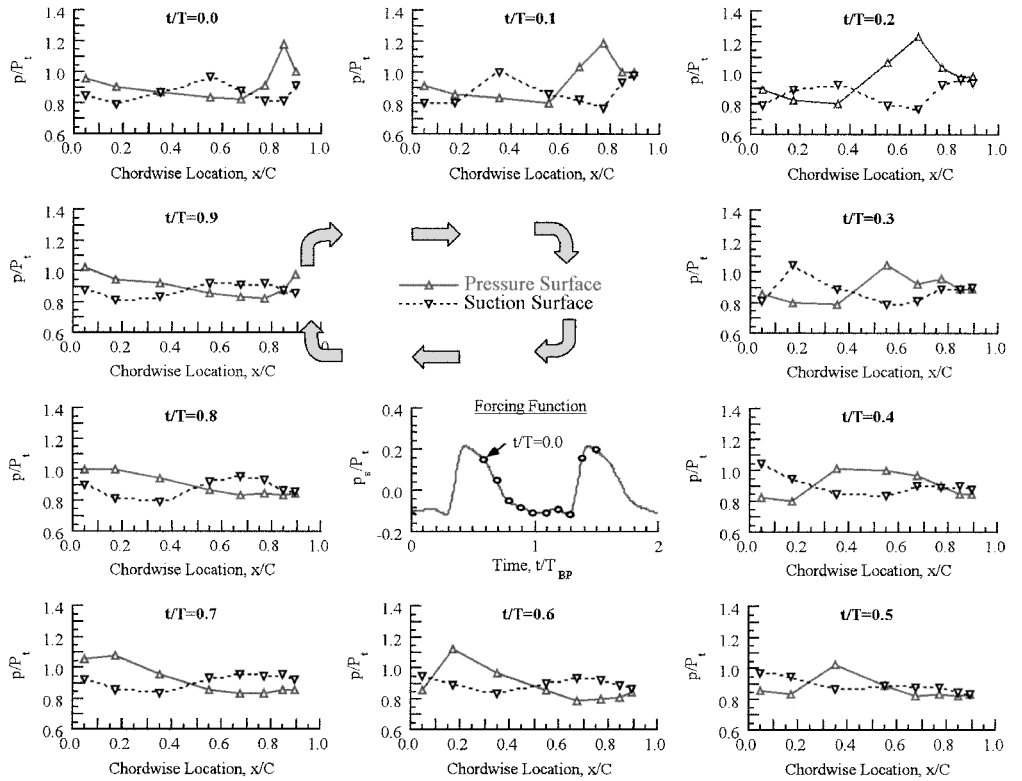

Fig. 10 Instantaneous IGV pressure distributions at 20,000 rpm (moderate axial spacing).

occur in the region aft of the reflection point ($p_3 > p_2$). Because the IGV flowfield is subsonic, a pressure wave is generated in the trailing-edge region that equalizes the pressure in the overpressure zone with the lower pressure region aft of the diffracted shock on the suction surface. This process is periodic because the shock waves translate with the rotor, with the reflection point moving upstream along the chord and the reflected shock segment continuing to propagate upstream toward the suction surface of the adjacent vane as the cycle progresses. As the reflection point moves past the nose of the airfoil, another pressure wave is generated in the leading-edge region to equalize the pressure on the upper and lower surfaces and the reflected shock segment is diffracted as it bends around the nose. Note that cascade effects can cause secondary reflections to occur, with the reflected shock segments impacting the surface of adjacent vanes or the multiple leading-edge shocks generated by the rotor as they propagate upstream. Particle image velocimetry (PIV) measurements of the vane-to-vane flow field currently in progress have verified this interaction process.[4]

The maximum pressure fluctuation associated with the rotor-generated forcing function occurs at time $t/T = 0.8$, whereas the vane response to this forcing function is first evident at $t/T = 0.9$. This time lag is caused by the rotor leading-edge shock waves being inclined to the axial direction, with the axial separation distance between the trailing-edge transducer and unsteady static pressure probe 31.4% vane chord. At time $t/T = 0.9$ the impact of the rotor shock causes an increase in the unsteady pressure surface loading in the trailing-edge region of the vane. Note that a suction surface response to the rotor shock is not yet evident at this time for the 90% chord transducer location because of the diffraction of the shock by the lower surface of the vane.

At the next time instant, the overpressure caused by the shock reflection on the pressure surface is clearly visible, with the suction surface of the vane also beginning to respond to the passing of the rotor shock. Note that the pressure surface loading decreases sharply aft of the reflection point, with the loading on both vane surfaces approaching the same value as the trailing edge is approached. Also, the unsteady loading generated by the reflected shock is very significant, with the maximum unsteady pressure difference across the vane nearly 50% of the time-average inlet total pressure.

As the reflection point moves upstream, the unsteady pressure surface loading aft of the reflection continues to increase to a maximum at time $t/T = 0.2$, after which it decreases and then remains about the same throughout the remainder of the cycle. This behavior is attributed to the decay of the incident shock waves as they interact with the upstream vane row and dissipate energy through the reflection and diffraction process. The reflected shocks, however, continue to propagate upstream as the cycle progresses. At time $t/T = 0.3$ the shock reflected by the pressure surface of the adjacent vane during the previous cycle has traveled across the vane passage and impacts the suction surface of the reference vane in the leading-edge region, causing the unsteady loading near 20% chord to increase noticeably.

Spectral Analysis

The phase-lock averaged rotor-generated forcing function and the resultant IGV unsteady aerodynamic response are decomposed into blade-pass frequency harmonics using a fast Fourier transform (FFT) algorithm, with the data window encompassing one complete rotor revolution. Figure 12 presents the spectral content of the forcing function at the moderate axial spacing for the transonic and subsonic rotor operating conditions. Six harmonics are required to describe the forcing function to the upstream IGV at the transonic design speed, with harmonics higher than this negligible as they are less than 0.5% of the inlet total pressure. These first six harmonics are quite large, with amplitudes of 15.1, 6.2, 2.7, 2.5, 1.3, and 0.7% of the inlet total pressure. Only three harmonics are required to describe the rotor-generated forcing function at the subsonic part-speed operating condition. These harmonics are much smaller than those at the transonic design speed, having amplitudes of 4.1, 1.0, and 1.1% of the inlet total pressure.

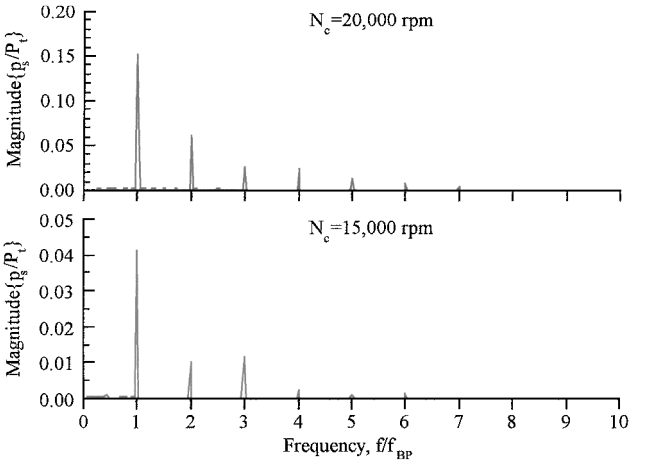

Fig. 12 Forcing function harmonic content (moderate axial spacing).

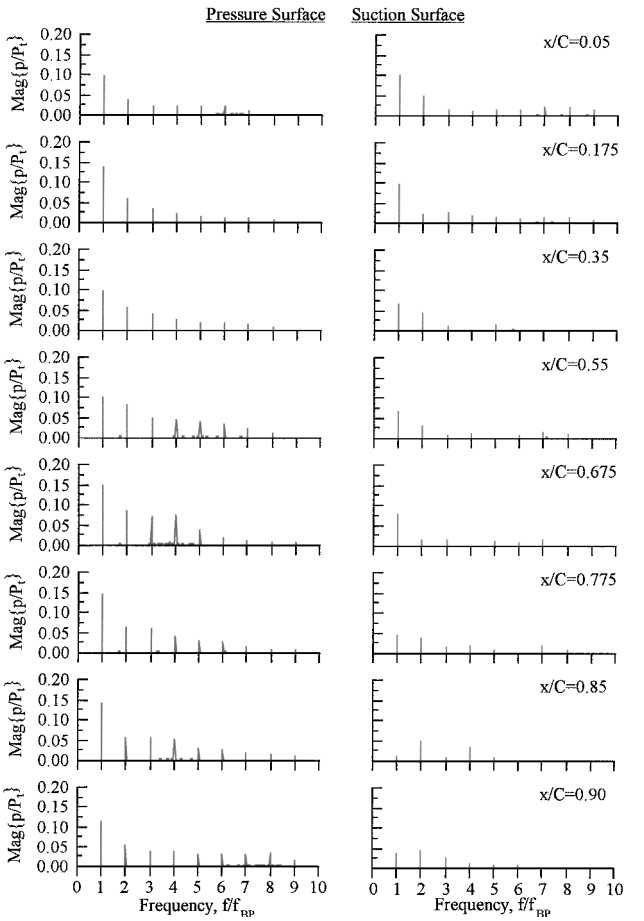

Fig. 13 IGV surface-pressure harmonic content at 20,000 rpm (moderate axial spacing).

Figures 13 and 14 show the harmonic content of the upstream IGV surface-pressure fluctuations corresponding to these forcing functions. At the transonic design speed there are several higher harmonics that were not present in the unsteady aerodynamic forcing function, most notably in the vane trailing-edge region on the pressure surface. This is indicative of nonlinear interactions caused by the reflection of the rotor shock by the vane pressure surface, with harmonics as high as 9 × band-pass filter (BPF) present in the vane response. These higher harmonics rapidly attenuate upstream, with the harmonic content on the pressure surface in the leading-edge region similar to that of the forcing function. Notice that the opposite trend occurs on the suction surface, with higher harmonics

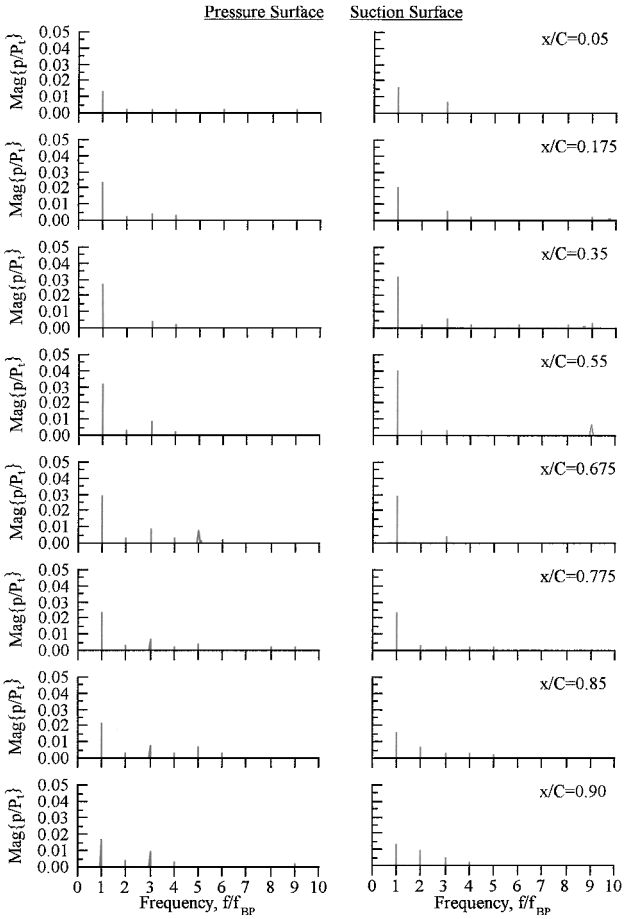

Fig. 14 IGV surface-pressure harmonic content at 15,000 rpm (moderate axial spacing).

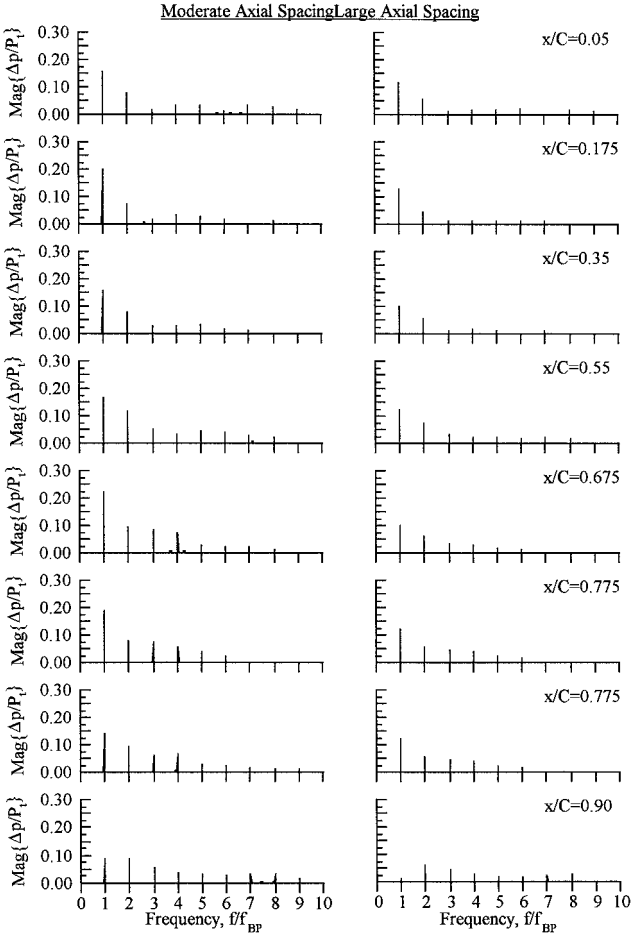

Fig. 15 IGV unsteady pressure difference harmonic content at 20,000 rpm.

present in the vane leading-edge region but not at the trailing edge. These higher harmonics are generated by the impact of the reflected shock segment with the vane suction surface near the leading edge.

At the subsonic rotor operating condition, the vane response is predominantly first harmonic (Fig. 14). Responses to the second and third harmonics of the forcing function are also present in the vane trailing-edge region, with the amplitudes of these higher harmonics rapidly attenuated upstream toward the leading edge. Note that for this operating condition the vane response spectrum correlates very well with that of the forcing function, indicating that the interactions are linear for subsonic rotor operation because of the rotor-generated forcing function having a much smaller amplitude at the part-speed operating condition.

The rotor-IGV interactions at the rotor transonic design speed are inherently nonlinear because of the high level of unsteadiness generated by the rotor shock system. To examine how these nonlinear interactions might impact forced response of the IGV, the harmonic content of the unsteady pressure difference, i.e., the unsteady aerodynamic loading, across the vane is examined. Figure 15 shows the unsteady pressure difference spectrum for the moderate and large axial spacings. Nonlinear effects are present at both axial spacings in the trailing-edge region, with several higher harmonics in the vane response that are not contained in the unsteady aerodynamic forcing function. Note that the unsteady loading at the trailing edge is very large at the moderate axial spacing, around 9% of the total pressure for the first two harmonics, 5.3% for the 3rd, and between 3–4% for the 4th–8th harmonics. Increasing the axial spacing causes the amplitude of the vane unsteady loading to attenuate slightly, but it is still very significant for the higher harmonics, ranging from 2–3% of the inlet total pressure for the 4th–8th harmonics.

It is not possible to eliminate all resonant crossings from the operating range of a turbomachine, particularly intersections of higher-order airfoil vibration modes with multiple harmonics of engine order excitations, i.e., 3 × BPF and higher. These higher-order vibration modes are usually characterized by edgewise bending patterns, with the thin trailing-edge region of the airfoil most susceptible to HCF failure.

These data show that blade-row interactions in the transonic flow regime cause significant unsteady loading in the trailing-edge region of the upstream vane row, with harmonics as high as 8 × BPF, a significant source of unsteady aerodynamic excitation to the vanes. Recall that the unsteady aerodynamic forcing function consisted only of the first six harmonics of blade-pass frequency, with the 4th–6th harmonics attenuating rapidly with increasing frequency. Thus, nonlinear interactions are responsible for the higher harmonics in the vane response, with these higher harmonics a significant source of unsteady aerodynamic excitation to the higher-order edgewise bending modes of vibration. Additionally, increasing the axial spacing did not significantly reduce the upstream vane trailing-edge loading for these higher harmonics. This indicates that simply increasing the IGV-rotor axial spacing will not alleviate the problem. Rather, design systems must account for nonlinear unsteady aerodynamic interactions when analyzing the forced response behavior of transonic stages.

Unsteady Aerodynamic Transfer Functions

The first harmonic unsteady aerodynamic transfer functions, i.e., the response nondimensionalized by the forcing function, are presented in Figs. 16–18. For a linear system these transfer functions should be identical for both axial spacings.

Figure 16 shows the amplitude and phase of the normalized pressure and suction surface responses at the transonic design speed. The agreement for both the magnitude and phase is very good along the entire vane pressure surface. The suction surface responses,

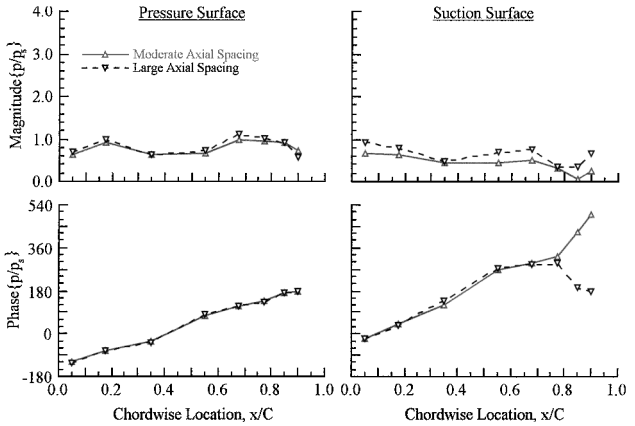

Fig. 16 Normalized first harmonic unsteady surface-pressure distributions at 20,000 rpm.

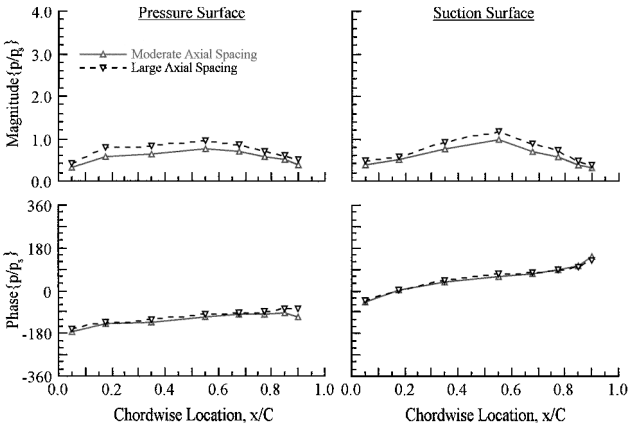

Fig. 17 Normalized first harmonic unsteady surface-pressure distributions at 15,000 rpm.

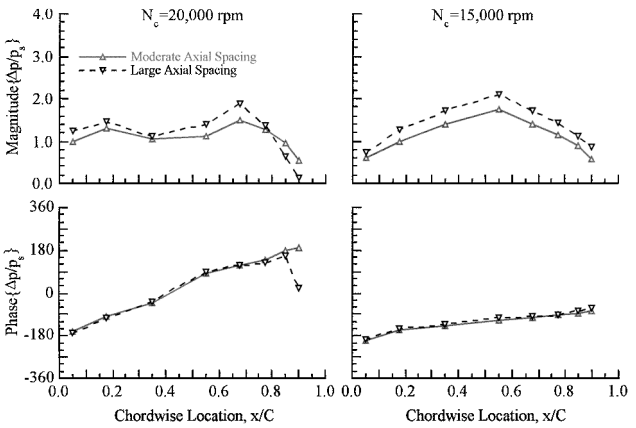

Fig. 18 Normalized first harmonic unsteady pressure difference distributions.

however, do not collapse for the two axial spacings. The magnitudes exhibit similar chordwise trends, but the nondimensional response for the moderate spacing is approximately 20% smaller. Additionally, the agreement in phase angle is excellent along the first 75% of the chord, but significant differences exist near the trailing edge. In fact, the phase angles over the aft 25% of the vane for the two axial spacings follow opposite trends, with this behavior attributed to nonlinear interactions. Note that the linear increase in phase angle indicates that disturbances propagate upstream along the vane. This trend is present on the pressure surface and the first 75% of the suction surface, adding further support to the conclusion that upstream propagating wave phenomena are present in the vane passage at the transonic operating condition. In addition, the magnitudes on both vane surfaces exhibit very similar characteristics to the numerical results of Eulitz et al.,[1] particularly that the location of the minimum response occurs near midchord on the pressure surface and near the trailing edge on the suction surface.

Figure 17 shows analogous results for the subsonic part-speed rotor operating condition. The trendwise agreement is excellent, but the magnitude and phase angle distributions for the two axial spacings are offset from one another. This trend is apparent on both vane surfaces, with the magnitude for the large axial spacing approximately 20–30% larger and the phase angle 5–10 deg greater across the entire chord. Note that the magnitude offset was also present in the data at the transonic design speed, being most noticeable on the suction surface. This offset may be caused by acoustic interactions between the IGV and rotor. Specifically, IGV-rotor interactions result in the generation of spinning acoustic modes at blade-pass frequency harmonics. Only certain of these modes are cut-on and propagate to the far field, with the cut-off modes decaying exponentially with axial distance. The unsteady static-pressure probe measurements include these interaction effects in addition to the forcing function generated by the rotor. Because the vane response is nondimensionalized by the forcing function, the offset may be caused by the presence of these interaction effects in the data. Note that the vane response may also be affected by these interactions, particularly by upstream propagating modes passing through the vane passage.

Figure 18 compares the nondimensional unsteady pressure difference across the vane for the transonic and subsonic rotor speeds. Consistent with the individual surface-pressure data, the nondimensional loading for the large axial spacing is approximately 25% larger and offset from that of the moderate axial spacing. At the transonic design speed this trend is present over the first 70% of the chord, with the magnitude and phase angle distributions very similar for both axial spacings. However, significant differences exist in the trailing-edge region because of nonlinear interaction effects. As the trailing edge is approached, the unsteady pressure difference appears to approach zero for both axial spacings, with the trailing-edge loading largest for the moderate axial spacing. The phase angles are also in excellent agreement over the first 85% chord, but differ by nearly 180 deg at the 90% chord transducer location. At the subsonic rotor operating condition these nonlinear interaction effects are not present, with the magnitude and phase angle distributions very similar for both axial spacings.

Conclusions

Unsteady aerodynamic interactions between the IGV and rotor of an advanced design transonic multistage compressor have been experimentally investigated, with the rotor-generated forcing function and resultant IGV response measured and analyzed at both design and part-speed operating conditions.

The unsteady static-pressure field generated by the rotor, i.e., the forcing function to the upstream IGV, was three-and-one-half times larger at the transonic design speed. The increase in unsteady aerodynamic loading on the upstream IGV as a result of this interaction was even more pronounced, being six times larger at the transonic design speed compared to the part-speed subsonic rotor operating condition. This dramatic increase in unsteady vane loading was attributed to nonlinear interaction effects caused by the high level of unsteadiness generated by the passing of the rotor shocks.

The impact of the rotor leading-edge shocks with the vane trailing edge resulted in the incident shock being reflected by the vane pressure surface and diffracted by the suction surface. The reflection point moved upstream as the cycle progressed, with the incident shock decaying as it propagated through the vane passage because of its interaction with the vane row. The reflected shock segment, however, traveled across the vane passage as it propagated upstream and eventually impacted the suction surface of the upper vane in the leading-edge region.

The unsteady aerodynamic loading on the vanes resulting from these transonic IGV-rotor interactions was very significant, with the maximum peak-to-peak static pressure fluctuations over the aft region of the vane as large as 60% of the inlet total pressure for the moderate axial spacing. Nonlinear interaction effects also introduced several higher harmonics into the vane response that were not present in the unsteady aerodynamic forcing function, with the pressure fluctuations on the vane aft region having components as high as 9 × BPF. These nonlinear interactions did not occur at the part-speed subsonic rotor operating condition, with both the forcing function and resultant vane response primarily first harmonic.

The higher harmonics generated by nonlinear interactions at the transonic design speed may be a significant source of forced response excitation to the vane, with the unsteady pressure difference amplitudes across the thin trailing edge ranging from 3–4% of the inlet total pressure for the 4th–8th harmonics. Increasing the IGV-rotor axial spacing did not alleviate this problem, with the higher harmonics attenuated only slightly. Thus, these higher harmonics may be a potential source of excitation to higher-order vibration modes that could lead to HCF failure of the thin trailing edges. Because it is impossible to eliminate all resonant crossings from the compressor operating range, design systems must account for these nonlinear interaction effects when analyzing the forced response behavior of transonic stages.

Acknowledgments

This research was sponsored by the Air Force Office of Scientific Research (AFOSR) and Pratt and Whitney. This support is most gratefully acknowledged.

References

[1] Eulitz, F., Engel, K., and Pokorny, S., "Numerical Investigation of Inviscid and Viscous Interaction in a Transonic Compressor," Propulsion and Energetics Panel 85th Symposium, AGARD-CP-571, Paper 38, May 1995.

[2] Liamis, N., Bacha, J. L., and Burgaud, F., "Numerical Simulations of Stator-Rotor Interactions on Compressor Blade Rows," Propulsion and Energetics Panel 85th Symposium, AGARD-CP-571, Paper 36, May 1995.

[3] Arnone, A., and Pacciani, R., "IGV-Rotor Interaction Analysis in a Transonic Compressor Using the Navier–Stokes Equations," *Journal of Turbomachinery*, Vol. 120, No. 1, 1998, pp. 147–155.

[4] Sanders, A. J., and Fleeter, S., "A PIV Investigation of IGV-Rotor Interactions in a Transonic Axial-Flow Compressor," AIAA Paper 99-2674, June 1999.